Vibrationally and Spin-Orbit-Resolved Inner-Shell X-ray Absorption Spectroscopy of the NH+ Molecular Ion: Measurements and ab Initio Calculations

Stéphane Carniato, Jean-Marc Bizau, Denis Cubaynes, Eugene Kennedy, Ségolène Guilbaud, Emma Sokell, Brendan Mclaughlin, Jean-Paul Mosnier

atoms

MDPI

Article

Vibrationally and Spin-Orbit-Resolved Inner-Shell X-ray Absorption Spectroscopy of the NH^+ Molecular Ion: Measurements and ab Initio Calculations

Stéphane Carniato [1], Jean-Marc Bizau [2,3], Denis Cubaynes [2,3], Eugene T. Kennedy [4], Ségolène Guilbaud [2], Emma Sokell [5], Brendan McLaughlin [6] and Jean-Paul Mosnier [4,*]

1 LCPMR, UMR 7614, Sorbonne Université Pierre et Marie Curie Campus, Université Pierre et Marie Curie, 4 Place Jussieu Barre 43-44, F-75005 Paris, France; stephane.carniato@upmc.fr
2 Institut des Sciences Moléculaires d'Orsay, CNRS, Université Paris–Sud, and Université Paris-Saclay, F-91405 Orsay, France; jean-marc.bizau@universite-paris-saclay.fr (J.-M.B.); denis.cubaynes@universite-paris-saclay.fr (D.C.); segolene.guilbaud@universite-paris-saclay.fr (S.G.)
3 Synchrotron SOLEIL, L'Orme des Merisiers, Saint-Aubin, BP 48, F-91192 Gif-sur-Yvette, CEDEX, France
4 School of Physical Sciences and National Centre for Plasma Science and Technology (NCPST), Dublin City University, Dublin 9, Ireland; eugene.kennedy@dcu.ie
5 School of Physics, University College Dublin, Belfield, Dublin 4, Ireland; emma.sokell@ucd.ie
6 Centre for Theoretical Atomic and Molecular Physics (CTAMOP), School of Mathematics and Physics, Queen's University Belfast, Belfast BT7 1NN, UK; bmcl104@gmail.com
* Correspondence: jean-paul.mosnier@dcu.ie

Received: 2 September 2020; Accepted: 29 September 2020; Published: 4 October 2020

Abstract: This article presents N^{2+} fragment yields following nitrogen K-shell photo-absorption in the NH^+ molecular ion measured at the SOLEIL synchrotron radiation facility in the photon energy region 390–450 eV. The combination of the high sensitivity of the merged-beam, multi-analysis ion apparatus (MAIA) with the high spectral resolution of the PLEIADES beamline helped to resolve experimentally vibrational structures of highly excited $[N1s^{-1}H]^{*+}$ electronic states with closed or open-shell configurations. The assignment of the observed spectral features was achieved with the help of density functional theory (DFT) and post-Hartree Fock Multiconfiguration Self-Consistent-Field/Configuration Interaction (MCSCF/CI) ab-initio theoretical calculations of the N1s core-to-valence and core-to-Rydberg excitations, including vibrational dynamics. New resonances were identified compared to previous work, owing to detailed molecular modeling of the vibrational, spin-orbit coupling and metastable state effects on the spectra. The latter are evidenced by spectral contributions from the $^4\Sigma^-$ electronic state which lies 0.07 eV above the NH^+ $^2\Pi$ ground state.

Keywords: NH^+; molecular ion; K-shell; merged-beam

1. Introduction

Small molecules and their cations, notably hydrides, play important roles in laboratory and astrophysical plasma processes [1] and in planetary atmospheric chemistry. Reliable data on their electronic and vibrational structures as well as their interaction with ionizing radiation are key for their identification in astrophysical environments and an understanding of their chemical reactivity [2]. Standard gas-phase chemistry models show that NH and NH^+ are present at various stages of the pathways to ammonia production in the interstellar medium [1–3]. NH has been observed in diffuse clouds [4], but laboratory observations only are known for NH^+. Amero and Vasquez [5] give a comprehensive experimental and theoretical review of the assignments of the observed bands in the NH^+ ultraviolet and visible spectra.

Photoionization studies in the inner-shell regime of neutral molecules of astrophysical interest are well-developed [6]. For the associated cations, however, largely due to experimental difficulties, similar photoionization studies have remained scarce. Hence, only in the past few years has the photo-ion merged-beam technique been successfully applied to several molecular hydride ions [7–11].

Recently, ion yields following X-ray absorption of the cationic series NHy^+ (y = 0–3) were measured and characteristic resonances in the energy range of the atomic nitrogen K-edge were identified by Bari et al. [12]. These authors reported marked changes in the energy of the observed resonances as a function of the number of hydrogen atoms bound to the central nitrogen atom. Theoretical modeling in the framework of molecular group theory was also performed by Bari et al. [12] for the electronic parts of the spectra in order to obtain line assignments.

In this work, we present new high-resolution measurements of the N^{2+} fragment yield following 1 s photo-absorption in the NH^+ molecular ion as a function of the photon energy near the nitrogen K-edge. We implement extended ab-initio theoretical methods to calculate both the electronic and vibrational parts of the N1s absorption spectrum of NH^+. The theoretical results are then compared with the experimental data to provide definitive spectral assignments for the observed resonance energies and a meaningful analysis of their intensity profiles, revealing the importance of vibrational and spin-orbit effects.

2. Experimental Details and Results

The experiments were carried out using the multi-analysis ion apparatus (MAIA), which is located at the SOLEIL synchrotron facility (high-resolution PLEIADES beam line). We only provide the important experimental points here (extensive details on MAIA can be found in Reference [13]). NH^+ ions were optimally produced by heating NH_3 gas in a 12.4 GHz electron cyclotron resonance ion source (ECRIS) with less than 1 mW of radiofrequency power. The ions were extracted at 4 kV and mass-selected by a dipole bending magnet. The resulting NH^+ beam was then merged with the counter-propagating, undulator-monochromatized, synchrotron radiation beam and the overlap between the two beams was optimized. NH^+ ion currents of ~140 nA were typically available in the overlap region. The fragments produced upon the photon–ion interactions were analyzed downstream according to their charge-to-mass ratio by another dipole magnet. The remaining parent NH^+ ions were collected in a Faraday cup while the ionization fragments were counted using microchannel plates. Only the N^{2+} fragmentation channel could be meaningfully measured during the experiments. N^+ and H^+ photo-fragment signals were never above the intense background noise produced by collisions between the fast NH^+ ion beam and the residual gas, despite a background pressure in the low 10^{-9} mbar range. Neutral fragments are not detectable in the MAIA apparatus.

Figure 1a,b present measurements of the variation of the relative cross-section for the production of N^{2+} photofragments as a function of the photon energy between 390 and 450 eV. The spectrum in Figure 1a was obtained with a photon bandwidth (BW) increasing from 220 meV at 390 eV to 250 meV at 450 eV photon energy. Figure 1b displays an enlargement of the 394–401 eV region recorded with a higher resolution bandwidth of 110 meV. The measured cross-sections were corrected for both variations of the NH^+ ion current and the photon flux, which were monitored with a Faraday cup and a calibrated SXUV 300 photodiode, respectively [13]. The statistical uncertainty is displayed on each experimental point using grey bars. Since the N^{2+} fragments are produced with some kinetic energy, the detection of all the fragments is not guaranteed and the cross-section for this fragmentation channel is obtained in arbitrary units only. The photon energy scale was calibrated on the excitation energy of the N^+ 1s → 2p photoexcitation lines [14] recorded during the same beamtime and corrected for the Doppler shift associated with the NH^+ ion velocity. The resulting uncertainty on the photon energy scale is ±40 meV.

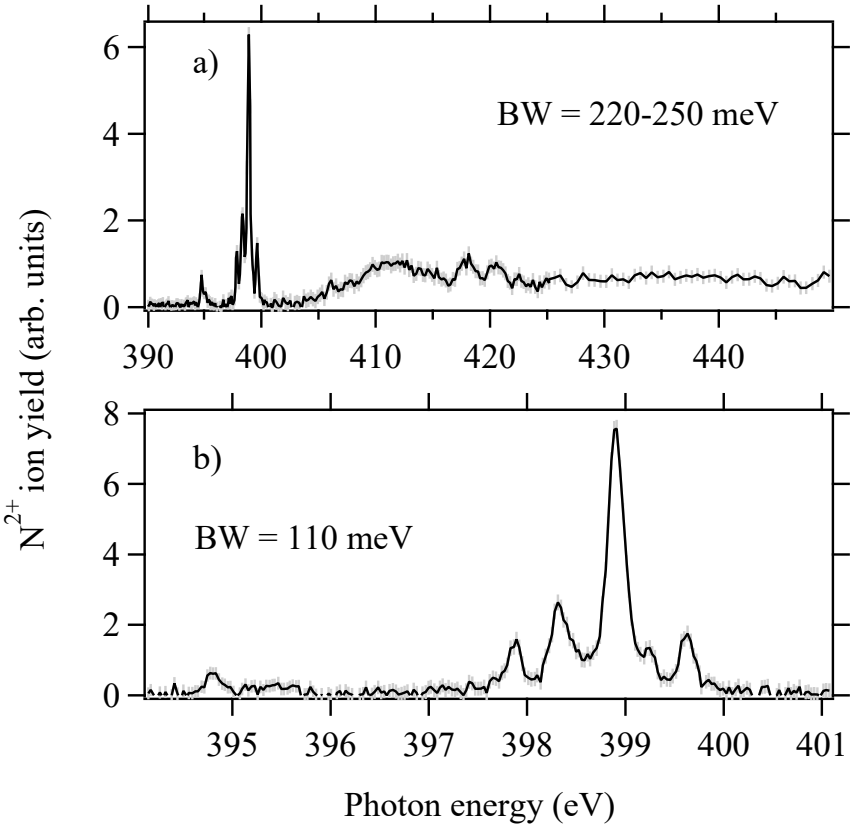

Figure 1. Experimental N^{2+} ion yield spectra of NH^+: (**a**) Recorded on the full photon energy range 390–450 eV with a photon bandwidth (BW) varying between 220 and 250 meV. (**b**) High-resolution spectrum obtained in the region 394–401 eV with a bandwidth of 110 meV.

Taking into account the difference in the photon energy resolution between the two experiments, generally good agreement on the position and shape of the structures is found with Bari et al.'s measurements [12]. The most noticeable difference lies in the relative intensity of the strong lines around 399 eV compared to the continuum above 425 eV.

3. Theoretical Aspects

3.1. Electronic Energies

The simulation of the X-ray absorption spectrum (XAS) of the NH^+ molecular ion consisted of computing the electronic transition energies and dipole moments associated with transitions between the quasi-degenerate fundamental ($^2\Pi$, $^4\Sigma^-$) electronic states and all core-excited states involved in the absorption process up to the $N1s^{-1}$ ionization thresholds. Excitation energies and oscillator strengths for the doublet and quartet states have been computed at both ($^2\Pi$, $^4\Sigma^-$) equilibrium geometries.

In order to calculate accurate energies of peaks in the N1s spectrum, full electronic relaxation energies (RE) with the departure of one N1s inner-shell electron and correlation energies at a post-Hartree-Fock (configuration interaction, CI) level of theory using single and double (SD) valence excitations (CI-SD) accompanying core-valence primary excitation were taken into account. Here, practically, the relaxation of the molecular orbitals (MOs) in the presence of a core vacancy was explicitly taken into account by using the Hartree-Fock Self Consistent Field (HF-SCF) approximation, which consists of a restricted open-shell Hartree-Fock calculation (ROHF) for the (low-lying) quartet core-ionized state $[N(1\sigma)^1 2\sigma^2\, 3\sigma^2 (1\pi_x)^1 (1\pi_y)^1]$, to ensure the degeneracy of the partially filled outermost π orbitals. This approach takes advantage of preparing a set of CI guesses for MOs where the valence-shell density contracts close to the (core) vacancy region.

Our methodology differs from the one adopted by Bari et al. [12], where the final states are described in a CI calculation employing the same orbitals as for the cationic initial state. As a remark, if the initial ground state is in principle correctly described, for the treatment of inner-shell excitations, CI calculations included all configurations that are constructed from the cationic reference configurations by promoting a single electron from the K shell to an unoccupied orbital, involving additional excitations of the valence electrons into virtual/singly occupied orbitals. However, including additional single valence excitations allow recovery of only part of the full relaxation and correlation is poorly described. Consequently, there is a certain imbalance in the description of initial and final electronic states. This imbalance can lead to a calculated transition energy which is slightly too low and varying relative shifts are necessary to be applied along the different orbital relaxation with respective excitation ranges.

Here, for the calculations of the first 100 low-lying core-excited energies, the [N$(1\sigma)^1 2\sigma^2$ $3\sigma^2(1\pi_x)^1(1\pi_y)^1$] molecular orbitals set were next employed within a Post-Hartree-Fock (HF) configuration interaction (CI) procedure, taking into account single and double substitutions (CI-SD) to virtual orbitals from the full valence (FV) manifold and a single hole (SH) in the core manifold (1 or 2 electrons in 1σ), using an iterative Davidson procedure developed by the main author of the present paper.

For the calculation of the oscillator strengths, the same set of MOs has been considered within a CI-SD (SH/FV-SD CI) approach for the description of the ground states of NH^+. This strategy ensures orthogonality of the spin-adapted configuration state functions (CSF) between the ground state and the core-excited states, which simplifies the calculation of the dipole transition moments. Of course, transition moments can be impacted by the description of the initial state. Otherwise, as a mirror to the strategy used by Bari et al. [12], the price to pay is that in principle, core-excitation energies are systematically overestimated by a few eV since the CI-SD ground state is constructed over relaxed core-excited molecular orbitals and not those of the real ground state. For that reason, excitation energies of the first low-lying states, i.e., the $^4\sum^-$ and $^4\Pi$ quartet states, were computed at the DFT level of theory using the Becke 3-parameter hybrid exchange [15] and the Lee-Yang-Parr (B3LYP) gradient-corrected correlation functional [16] with the general atomic and molecular electronic structure system GAMESS (US) quantum chemistry package [17]. These values are considered as energies of reference for prior calibration of the theoretical spectrum. Finally, spin-orbit coupling was also considered. The Breit-Pauli operator was used as implemented in the GAMESS (US) package in order to reveal the key spin-orbit components in the spectrum.

In summary, whatever the two approaches, this balance problem (using either initial MOs or relaxed MOs) is strongly related to the CI approach itself that considers a unique guess of MOs which are not optimal for the description of all of the states of the spectrum.

3.2. Vibrational Analysis, Potential Energy Curves

Assuming that the N K-hole lifetime width is similar to that measured in the nitrogen molecule (105 meV [18]), and because the monochromator bandwidth used in the present measurements was as low as 110 meV, several fine-structure features attributable to vibrational and/or initial population effects were observed in the spectra. In order to take into account the vibrational effects in the core-excited spectra, DFT/B3LYP equilibrium geometries and low-lying one-dimensional potential energy curves (PEC) of the initial and core-excited states of NH^+ have been calculated.

As reported in previous studies (see, for example, Reference [5] and references therein), the electronic ground state of the NH^+ molecular ion is a $^2\Pi$ doublet with seven electrons forming the $1\sigma_{1s}^2\ 2\sigma^2\ 3\sigma^2\ 1\pi^1$ electronic configuration. A quartet open-shell $^4\Sigma^-$ ($1\sigma_{1s}^2\ 2\sigma^2\ 3\sigma^1\ 1\pi^2$) electronic state is quasi-degenerate with the fundamental state as it lies only 0.07 eV above the $^2\Pi$ state. Consequently, both these configurations must be considered in order to properly describe the experiments. PECs of the $^2\Pi$ and the $^4\sum^-$ ground states were simulated at a Multiconfiguration Self-Consistent-Field (MCSCF) level of theory as implemented in the GAMESS (US) package. Practically, the two N1s

inner-shell electrons ($N1\sigma^2$) have been frozen. The MCSCF expansions comprise single (S) up to double (D) substitutions out of each of the restricted open-shell Hartree-Fock (ROHF) reference configurations. The reference active-space (26 molecular orbitals) includes here the 2σ, 3σ, $1\pi_x$, $1\pi_y$ (five electrons) outermost occupied and the twenty-two lowest-lying unoccupied molecular orbitals. In order to evaluate the energy spacing between the $^2\Pi$ and $^4\sum^-$ potential energy curves, DFT/B3LYP geometry optimizations and frequency calculations have been performed.

In order to determine the vibrational progression and Frank-Condon factors (FC) associated with the most relevant electronic transitions emerging from the x-ray absorption (XAS) N1s inner-shell spectrum of NH^+, the PEC of selected low-lying N1 s^{-1} core-excited states of interest have been calculated for internuclear distances ranging between 0.6 and 5 Å and are displayed in Figure 2 for the internuclear distance region between 0.6 and 3 Å.

In practice, we used the ROHF molecular orbitals of the $N1s^{-1}\,^4\Sigma^-$ quartet low-lying state computed for each interatomic distance. For each distance, a CI-SD calculation was performed with the occupation Restricted Multiple Active Space (ORMAS) method implemented in the GAMESS (US) package, in which the six valence electrons and one N1s inner-shell electron were explicitly correlated at a moderate cost, including up to 65 active molecular orbitals in order to collect the first PECs of the $[N1s^{-1}\ H]^+$ core-excited configurations with $^2\Delta$, $^2\Sigma^+$, $^{2,4}\Sigma$, $^{2,4}\Pi$ symmetries, generating ~7×10^6 configuration state functions (CSF).

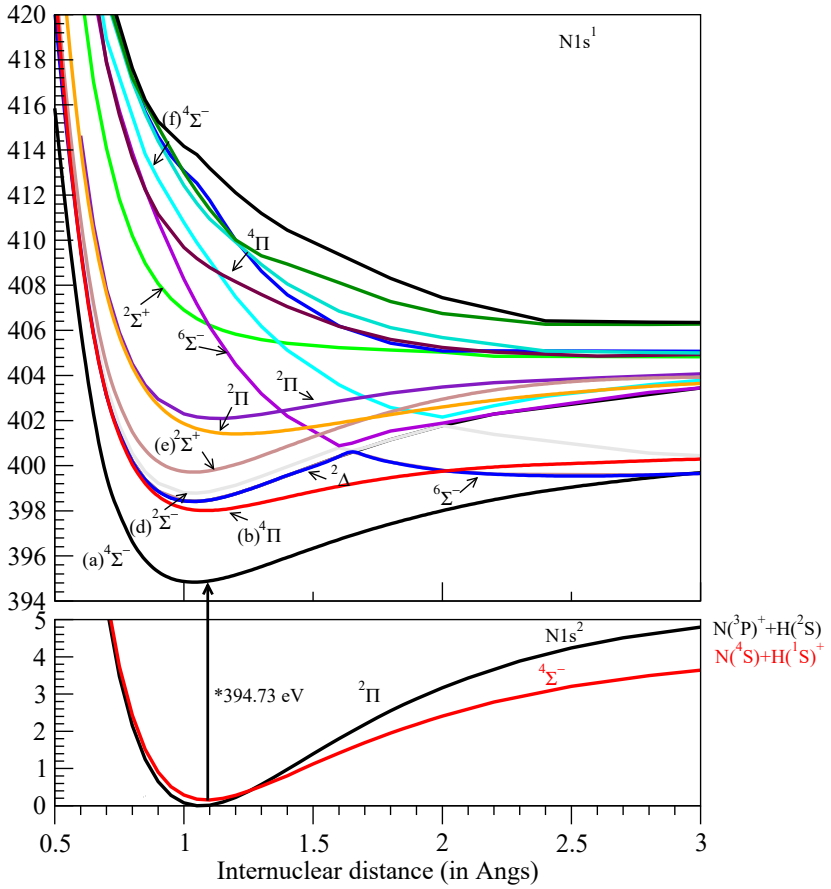

Figure 2. Multiconfiguration Self-Consistent Field (MCSCF) $N1s^2$ doublet $^2\Pi$ and quartet $^4\Sigma^-$ ground states (lower panel) and low-lying configuration interaction single and double substitutions (CI-SD) $N1s^1$ nitrogen K-shell (upper panel) potential energy curves of the NH^+ molecular ion. * The bottom of the lowest $N1s^{-1}\,^4\Sigma^-$ potential energy curve is set to the vertical density functional theory (DFT) energy transition of 394.73 eV represented by the vertical arrow (see text).

As the CI guess of MOs used to describe all the core-excited states is based on the single N1s^{-1} $^4\Sigma^-$ configuration, the CI-SD energy gap between the low-lying state $^4\Sigma^-$ state and the higher states can be overestimated, but the spacing between them can be expected to be satisfactory. In order to reproduce with accuracy the gap between the $^4\Sigma^-$ and the first $^4\Pi$ core-excited state, we performed two single points ($^4\Sigma^-$ and $^4\Pi$) of energy at a larger CI-SDT level, generating ~10^8 CSFs. A global shift of all the core-excited states above $^4\Sigma^-$ was assumed using this new gap value to compare theory vs experiments.

All the calculations were realized with the large aug-cc-pCV5z basis set [19] on all atoms augmented by additional (4s/4p/2d/2f) diffuse functions.

The eigenvalue/eigenfunction problem for the stretching motion taking into account vibrational effects was then solved using the one-dimensional Hamiltonian model that can be written as

$$H = \frac{-\hbar^2}{2\mu}\frac{d^2}{dr^2} + V(r) \tag{1}$$

where μ is the reduced mass of the system, r is the internuclear distance, and $V(r)$ is the molecular potential. The eigenvectors (vibrational wave functions) and eigenvalues (vibrational levels) were obtained by diagonalizing the Hamiltonian in a tridiagonal form using the finite difference approximation and a cubic spline interpolation of the potential energy curves. The matrix elements are

$$H_{i,j} = \frac{-\hbar^2}{2\mu\Delta^2}\left(2\delta_{i,j} - \delta_{i-1,j} + \delta_{i+1,j}\right) + V(r)\delta_{i,j} \tag{2}$$

where Δ is the uniformly spaced mesh. The fundamental frequency (ω_e) and anharmonicity constant (x_e), commonly expressed in terms of the vibrational expression

$$G_v = \omega_e\left(\upsilon + \frac{1}{2}\right) - \omega_e x_e\left(\upsilon + \frac{1}{2}\right)^2, \tag{3}$$

were derived for the ground state and core-excited states of interest in the present study, where υ is the vibrational quantum number.

3.3. Absorption Cross-Section Spectrum

The absorption spectrum was obtained by convolving the mean value of the dipole transition moment for randomly orientated molecular ions in the gas phase, computed at the equilibrium geometry of the system in its ground state, with a Voigt profile which accounts for both the lifetime and instrumental broadenings. The lifetime broadening was assumed to be independent of both core-excited electronic states and the internuclear distance. The transition moments $\mu_{i\to f}$ and the cross-sections were evaluated in the length gauge as follows:

$$\overline{\sigma}_{i\to f}(\omega) = \frac{4}{3}\frac{\pi^2 e^2\hbar}{(4\pi\varepsilon_o)mc}\frac{\left(E_f - E_i\right)^2 m}{\hbar^3\omega}\,\mu^2_{i\to f}\,\delta\left(\omega - \omega_{fi}\right) = \frac{2}{3}\frac{\left(E_f - E_i\right)^2 m}{\hbar^3\omega}\mu^2_{i\to f}\,C\,\delta\left(\omega - \omega_{fi}\right) \tag{4}$$

where ω is the photon frequency, $\delta\left(\omega - \omega_{fi}\right) = \frac{\gamma}{2\pi\left[(\omega-\omega_{fi})^2 + \frac{1}{4}\gamma^2\right]}$ is the Lorentzian line shape, $\frac{2}{3}\frac{\left(E_f - E_i\right)^2 m}{\hbar^3\omega}\mu^2_{i\to f}$ is the oscillator strength averaged over all possible molecular orientations, and

$$C = \frac{2\pi^2 e^2\hbar}{(4\pi\varepsilon_o)mc} = 109.8 \text{ Mb eV}.$$

The N1s^{-1} spectrum of the NH^+ molecular ion was simulated using a Voigt profile, where γ is the full width at half maximum (FWHM) of the Lorentzian profile corresponding to the N1s^{-1} core-hole lifetime (γ = 105 meV) and a Gaussian function with FWHM equal to ξ = 110 meV to simulate the

experimental broadening. It should be noted that the experimental spectral bandwidth in the higher photon energy was greater (220–250 meV), but in this region, no individual lines are resolved, several of the upper states involved are strongly dissociative, and using the smaller bandwidth for the theoretical spectrum does not affect the simulation. Finally, the average cross-section for a photon of energy ω' is given by

$$\overline{\sigma}(\omega') = \sum_{f=1}^{n} \int \overline{\sigma}_{i\to f}(\omega) \frac{2\sqrt{ln2}}{\xi\sqrt{\pi}} e^{-4ln2\ (\omega'-\omega)^2/\xi^2}\, d\omega \quad (5)$$

where n is the number of final electronic states.

4. Results and Discussion

4.1. Ground States

Both the vibrational frequencies and the equilibrium distances of the quasi-degenerate electronic ground states are key parameters in order to calculate the N1s spectrum of NH^+. The calculated values for the ($^2\Pi$) and ($^4\Sigma^-$) ground states are given in Table 1 and compared to available experimental values [20].

Table 1. NH^+ calculated internuclear distances, d_{NH}, and frequencies, ν_{NH}, for the $^2\Pi$ and $^4\Sigma^-$ ground states compared to experiments (Reference [20]) for the $N1s^{-1}$ core-excited states located in the 394–400 photon energy region (see text).

Main Configuration	State	d_{NH} (Å)	ν_{NH} (cm^{-1})	Type [1]
$1\sigma_1{}^2 2\sigma^2 3\sigma^2 3p_{x,y}{}^1$	$^2\Pi$	1.0776	2974.3	DFT/B3LYP
		1.065	3064.2	MCSCF
		1.0692	3047.58	Experimental value from Ref. [20]
$1\sigma_1{}^2 2\sigma^2 3\sigma^1 3p_x{}^1 3p_y{}^1$	$^4\Sigma^-$	1.1135	2502.0	DFT/B3LYP
		1.096	2716.0	MCSCF
		1.093	2672.57	Experimental value from Ref. [20]
$1\sigma_1{}^1\ 2\sigma^2 3\sigma^2 3p_x{}^1 3p_y{}^1$	$^4\Sigma^-$	1.0341	3169.0	DFT/B3LYP
		1.040	3182.0	CI-SD
$1\sigma_1{}^1 2\sigma^2 3\sigma^1 3p_x{}^2 3p_y{}^1/3p_x{}^1 3p_y{}^2$	$^4\Pi$	1.0919	2517.0	DFT/B3LYP
		1.082	2557.0	CI-SD
$1\sigma_1{}^1 2\sigma^2 3\sigma^2 3p_x{}^2 3p_y{}^0/3p_x{}^0 3p_y{}^2$	$^2\Delta$	1.0371	3140.0	DFT/B3LYP
		1.035	3250	CI-SD
$1\sigma_1{}^1 2\sigma^2 3\sigma^2 3p_x{}^1 3p_y{}^1$	$^2\Delta$	1.035	3250.0	CI-SD

[1] Definition of acronyms: density functional theory/Becke 3-parameter hybrid exchange and Lee-Yang-Parr gradient-corrected correlation functional (DFT/B3LYP); Multiconfiguration Self-consistent Field (MCSCF); Configuration interaction with single and double substitutions (CI-SD).

For the $^2\Pi$ state, the dissociation energy (D_o = 4.98 eV), equilibrium distance, R_e, and the fundamental vibrational frequency, ω_e, are fairly well reproduced by the present MCSCF-SD calculations compared to the most accurate calculated data (R_e = 1.0687 Å, ω_e = 3052.9 cm^{-1}, D_o = 4.64 eV [21]) and experimental data (D_o = 4.66 eV, R_e = 1.077 Å, ω_e = 2980.65 cm^{-1} [22], or see also Reference [5] and references therein). The calculation of the anharmonicity coefficient from the PEC analysis gives $\omega_e x_e$ = 73.0 cm^{-1}.

For the quartet $^4\sum^-$ state, the MCSCF dissociation energy (D_o = 3.50 eV), equilibrium distance (R_e = 1.096 Å), and fundamental vibrational frequency (ω_e = 2716 cm^{-1}) are also well reproduced by our theoretical calculations compared to experimental data (D_o = 3.33 eV, R_e = 1.093 Å, ω_e = 2652.29 cm^{-1} [5,20]). In this case, the anharmonicity coefficient is $\omega_e x_e$ = 81 cm^{-1}.

In order to evaluate the energy gap between the $^2\Pi$ and $^4\sum^-$ potential energy curves, which is a key parameter for the analyses of the experimental data, DFT/B3LYP geometry optimizations and frequency calculations were performed (see Table 1). For the doublet, the equilibrium distance and ω_e were estimated to be 1.0776 Å and 2974 cm^{-1}, respectively. For the quartet, the DFT equilibrium distance and the harmonic frequency are estimated to be 1.113 Å and 2502 cm^{-1} respectively, in excellent agreement with MCSCF-SD and experimental values [22]. The calculated DFT adiabatic electronic energy gap between the $^2\Pi$ and the $^4\sum^-$ states is estimated to be 0.166 eV. Considering the zero-point energy correction, the vibrational corrected energy gap is finally found equal to 0.137 eV at DFT and 0.143 eV at MCSCF level of theories, somewhat overestimating the experimental value (0.071 eV).

4.2. Core-Excited States

The NH^+ experimental ion yield spectrum covering the full energy window is shown in Figure 1a. Mainly, three distinctive regions are observed: (i) the first region presents a single weak structure close to 395 eV, (ii) the second region is located around 397–400 eV, showing four well-defined components. A high-resolution spectrum of this region is displayed in Figure 1b. (iii) Above 405 eV, the spectrum consists of broad and unresolved features, likely due to the excitation of a 1 s electron to higher empty orbitals, to form Rydberg series converging to the 1 s^{-1} ionization thresholds around 425–430 eV.

In the following, we will separately discuss the three regions. The results of our calculations for the three regions are reported in Table 2.

4.2.1. Region 394–396 eV (Peaks a $^4\Sigma^-$)

The energy position of the low-lying structure (see Figure 1a,b and Figure 3), labeled a, is measured at 394.81 (6) eV. The DFT/B3LYP vertical electronic transition energy is estimated to be 394.53 eV and corresponds to a solely electronic excitation from the N1s inner-shell to the 3σ singly occupied molecular orbital to form the final $^4\Sigma^-$ quartet open-shell N1$\sigma^1$2$\sigma^2$3$\sigma^2$1$\pi_x{}^1$1$\pi_y{}^1$ electronic configuration, in agreement with Bari et al. [12]. This assignment is confirmed by analysis of the PEC displayed in Figure 2 showing that the low-lying potential energy curve is well associated with the $^4\Sigma^-$ quartet which dissociates into the N(^{4}S) + H$^+$(^{1}S) final products.

The adiabatic DFT/B3LYP optimized equilibrium distance experiences a substantial shrink by 0.1 Å (R = 1.034 Å) with respect to the quartet ground state PEC of NH^+. This relatively large contraction of the NH bond is corroborated by CI-SD calculations, for which the minimum of the PEC is found at nearly 1.040 Å. The MCSCF numerical vibrational frequency is equal to 3182 cm^{-1}, i.e., ≈470 cm^{-1} larger than for the $^4\sum^-$ quartet electronic ground state. The anharmonicity coefficient $\omega_e x_e$ extracted from PEC analysis is ≈87 cm^{-1}.

Taking into account the differential zero-point energy correction between the initial and final states (MCSCF: +0.03 eV, DFT: +0.04 eV) and the relativistic correction (+0.2 eV) due to departure of one N1s inner-shell electron, the corrected DFT vertical core-excitation energy is finally found at 394.77 eV, in excellent agreement with the experimental data. The CI-SD calculated oscillator strength for the $^4\Sigma^- \rightarrow {}^4\Sigma^-$ transition (peak a) is evaluated to be 0.043, corresponding to a strength of 4.72 Mb eV.

In spite of the weak signal, the band presents an asymmetric tail extending up to ≈395.5 eV (see Figure 1a). As clearly shown by theory, the reason for such asymmetry on the high-energy tail of the peak is due to a vibrational progression. Our simulation shows that the vibrational progression is due to the net shortening of the N-H bond in the N1s core hole state compared to the ground state. The vibrational profile exhibits two significant components with relative intensities 0.82:0.17, lying at 0.19 eV (v = 0→v′ = 0, band a) and 0.56 eV (v = 0→v′ = 1, band a′) above the PEC adiabatic minimum, respectively. Considering the zero-point energy correction of 0.04 eV (at the DFT level of theory) for the $^4\Sigma^- \rightarrow {}^4\Sigma^-$ transition, the energy positions of the theoretical bands a and a′ are finally calculated to be 394.77 eV and 395.14 eV, respectively, in good agreement with the experimental data.

Table 2. Configuration interaction with single and double substitutions (CI-SD) from the full valence manifold results for vertical transitions of valence character from the density functional theory (DFT) doublet (R_e = 1.077Å) and quartet (R_e = 1.113 Å) optimized ground state geometries. Main configurations and weights (W) in %, measured (E_{mea}) and calculated (E_{cal}) transition energies in eV, oscillator strengths f_{theo} above 0.001 only are reported, and labels used to identify the present experimental data. For doublet states, f_{theo} have been calculated for only one (x or y) component.

Electronic Transition	Final State	E_{mea} (eV) [1]	E_{cal} (eV)	W (%)	f_{theo}	Label
Region1						
$1\sigma^2 2\sigma^2 3\sigma^1 1\pi_x^1 1\pi_y^1 \rightarrow 1\sigma^1 2\sigma^2 3\sigma^2 1\pi_x^1 1\pi_y^1$	$^4\Sigma^-$	394.81(6)	394.73 [2]	98.0	0.0430	a
Region2						
$1\sigma^2 2\sigma^2 3\sigma^1 1\pi_x^1 1\pi_y^1 \rightarrow 1\sigma^1 2\sigma^2 3\sigma^1 1\pi_{x(y)}^1 1\pi_{y(x)}^2$	$^4\Pi$	397.87(5)	397.84 [3]	95.6	0.1560	b
$1\sigma^2 2\sigma^2 3\sigma^2 1\pi_{x(y)}^1 \rightarrow 1\sigma^1 3\sigma^2 1\pi_{x(y)}^2 \pi_{y(x)}^0$	$^2\Delta$	398.31(6)	398.40 [4]	98.7	0.0401	c
$1\sigma^2 2\sigma^2 3\sigma^2 1\pi_{x(y)}^1 \rightarrow 1\sigma^1 2\sigma^2 3\sigma^2 1\pi_x^1 \pi_y^1$	$^2\Delta$	398.46(11)	398.40	98.7	0.0401	c′
$1\sigma^2 2\sigma^2 3\sigma^2 1\pi_{x(y)}^1 \rightarrow 1\sigma^1 2\sigma^2 3\sigma^2 1\pi_x^1 \pi_y^1$	$^2\Sigma^-$	398.91(4)	398.70	98.7	0.1208	d
$1\sigma^2 2\sigma^2 3\sigma^2 1\pi_{x(y)}^1 \rightarrow 1\sigma^1 2\sigma^2 3\sigma^2 1\pi_{x(y)}^2 \pi_{y(x)}^0$	$^2\Sigma^+$	399.63(5)	399.63	92.5	0.0385	e
Region 3						
$1\sigma^2 2\sigma^2 3\sigma^1 1\pi_x^1 1\pi_y^1 \rightarrow 1\sigma^1 2\sigma^2 3\sigma^1 1\pi_x^1 1\pi_y^1 4\sigma^1$	$^4\Sigma^-$		409.04	88.0	0.0332	f
$1\sigma^2 2\sigma^2 3\sigma^1 1\pi_x^1 1\pi_y^1 \rightarrow 1\sigma^1 2\sigma^1 3\sigma^2 1\pi_{x(y)}^2 1\pi_{y(x)}^1$	$^4\Pi$		409.14	74.0	0.0012	g
$1\sigma^2 2\sigma^2 3\sigma^2 1\pi_{x(y)}^1 \rightarrow 1\sigma^1 2\sigma^2 3\sigma^2 1\pi_{x(y)}^1 4\sigma^1$	$^2\Pi$		412.17	85.0	0.0261	h
$1\sigma^2 2\sigma^2 3\sigma^1 1\pi_x^1 1\pi_y^1 \rightarrow 1\sigma^1 3\sigma^1 1\pi_x^1 1\pi_y^1 4\sigma^1$	$^4\Sigma^-$		412.20	77.8	0.0078	i
$1\sigma^2 2\sigma^2 3\sigma^1 1\pi_x^1 1\pi_y^1 \rightarrow 1\sigma^1 3\sigma^1 1\pi_x^1 1\pi_y^1 4\sigma^1$	$^4\Sigma^-$		412.40	80.6	0.0189	j
$1\sigma^2 2\sigma^2 3\sigma^2 1\pi_{x(y)}^1 \rightarrow 1\sigma^1 2\sigma^2 3\sigma^2 1\pi_{x(y)}^1 4\sigma^1$	$^2\Pi$		414.00	57.8	0.0032	k
$1\sigma^2 2\sigma^2 3\sigma^1 1\pi_x^1 1\pi_y^1 \rightarrow 1\sigma^1 3\sigma^1 1\pi_x^1 1\pi_y^1 5\sigma^1$	$^4\Sigma^-$		414.67	89.2	0.0039	l
$1\sigma^2 2\sigma^2 3\sigma^1 1\pi_x^1 1\pi_y^1 \rightarrow 1\sigma^1 3\sigma^1 1\pi_x^1 1\pi_y^1 2\pi_{x(y)}^1$	$^4\Pi$		414.70	59.6	0.0174	m
$1\sigma^2 2\sigma^2 3\sigma^2 1\pi_x^1 \rightarrow 1\sigma^1 2\sigma^2 3\sigma^1 1\pi_x^1 \pi_y^1 4\sigma^1$	$^2\Sigma^-$		414.80	82.0	0.0015	n
$1\sigma^2 2\sigma^2 3\sigma^2 1\pi_{x(y)}^1 \rightarrow 1\sigma^1 2\sigma^2 3\sigma^2 1\pi_{x(y)}^1 4\sigma^1$	$^2\Pi$		415.95	57.8	0.0053	o
$1\sigma^2 2\sigma^2 3\sigma^2 1\pi_x^1 \rightarrow 1\sigma^1 2\sigma^2 3\sigma^1 1\pi_x^1 \pi_y^1 4\sigma^1$	$^2\Delta$		416.09	78.8	0.0015	p
$1\sigma^2 2\sigma^2 3\sigma^2 1\pi_x^1 \rightarrow 1\sigma^1 2\sigma^2 3\sigma^1 1\pi_{x(y)}^2 \pi_{y(x)}^0 4\sigma^1$	$^2\Delta$		416.09	78.8	0.0015	p′
$1\sigma^2 2\sigma^2 3\sigma^2 1\pi_x^1 \rightarrow 1\sigma^1 2\sigma^2 3\sigma^1 1\pi_x^1 \pi_y^1 4\sigma^1$	$^2\Sigma^-$		416.51	76.9	0.0032	q
$1\sigma^2 2\sigma^2 3\sigma^2 1\pi_x^1 \rightarrow 1\sigma^1 2\sigma^2 3\sigma^1 1\pi_{x(y)}^2 1\pi_{y(x)}^0 4\sigma^1$	$^2\Sigma^+$		417.68	50.1	0.0016	r
$1\sigma^2 2\sigma^2 3\sigma^2 1\pi_{x(y)}^1 \rightarrow 1\sigma^1 2\sigma^2 3\sigma^2 1\pi_{x(y)}^1 4\sigma^1$	$^2\Pi$		418.07	77.4	0.0040	s
$1\sigma^2 2\sigma^2 3\sigma^1 1\pi_x^1 1\pi_y^1 \rightarrow 1\sigma^1 3\sigma^1 1\pi_x^1 1\pi_y^1 3\pi_{x(y)}^1$	$^4\Pi$		418.01	94.5	0.0013	t
$1\sigma^2 2\sigma^2 3\sigma^2 1\pi_x^1 \rightarrow 1\sigma^1 2\sigma^2 3\sigma^2 1\pi_x^1 2\pi_y^1$	$^2\Sigma^-$		418.14	76.9	0.0012	u
$1\sigma^2 2\sigma^2 3\sigma^1 1\pi_x^1 1\pi_y^1 \rightarrow 1\sigma^1 3\sigma^1 1\pi_x^1 1\pi_y^1 3\pi_{x(y)}^1$	$^4\Sigma^-$		418.19	53.5	0.0026	v
$1\sigma^2 2\sigma^2 3\sigma^2 1\pi_x^1 \rightarrow 1\sigma^1 2\sigma^2 3\sigma^2 1\pi_x^1 2\pi_y^1$	$^2\Delta$		418.61	76.9	0.0013	x
$1\sigma^2 2\sigma^2 3\sigma^2 1\pi_x^1 \rightarrow 1\sigma^1 2\sigma^2 3\sigma^2 1\pi_x^1 2\pi_x^1$	$^2\Delta$		418.61	76.9	0.0013	x′
$1\sigma^2 2\sigma^2 3\sigma^1 1\pi_x^1 1\pi_y^1 \rightarrow 1\sigma^1 3\sigma^1 1\pi_x^1 1\pi_y^1 2\pi_{x(y)}^1$	$^4\Pi$		419.55	84.5	0.0027	y
$1\sigma^2 2\sigma^2 3\sigma^1 1\pi_x^1 1\pi_y^1 \rightarrow 1\sigma^1 3\sigma^1 1\pi_x^1 1\pi_y^1 5\sigma^1$	$^4\Sigma^-$		419.76	51.3	0.0062	z
$1\sigma^2 2\sigma^2 3\sigma^2 1\pi_x^1 \rightarrow 1\sigma^1 2\sigma^2 3\sigma^1 1\pi_x^1 1\pi_y^1 5\sigma^1$	$^2\Sigma^-$		420.18	69.0	0.0020	za
$1\sigma^2 2\sigma^2 3\sigma^1 1\pi_x^1 1\pi_y^1 \rightarrow 1\sigma^1 3\sigma^1 1\pi_x^1 1\pi_y^1 2\pi_{x(y)}^1$	$^4\Pi$		420.27	81.7	0.0099	zb

[1] The number in brackets is the uncertainty on the last digit. [2] Vertical relativistic density functional theory (DFT) value (394.73 eV) corrected by zero-point energy (0.02 eV) used as reference. [3] Vertical transition energy value at 1.096 Å (Multiconfiguration self-consistent Field (MCSCF) minimum distance of the $^4\Sigma^-$ ground state) deduced from Figure 2. [4] Doublet vertical transition energy value at 1.065 Å (Multiconfiguration self-consistent Field (MCSCF) local minimum of the $^2\Pi$ ground state) deduced from Figure 2. 394.77 eV and 395.14 eV, respectively, in good agreement with experimental data.

The presence of the $^4\Sigma^- \rightarrow {}^4\Sigma^-$ transition in the spectrum is due to the plasma source conditions, since the ground electronic state is formally a $^2\Pi$ state, as stated in previous works (see Reference [19] and references therein) and confirmed here by the present calculations, and lies only ≈0.1 eV below the $^4\sum^-$ state. The time of flight of the ions between the source and the interaction region is of the order of a few μ-seconds and, thus, a fraction of the ions interacting with the photons may be vibrationally and/or electronically excited, particularly in a relatively long-lived, low-lying state such as the $^4\Sigma^-$.

4.2.2. Region 397–400 eV

A fitting by Voigt profiles of the experimental data displayed on Figure 3a shows the seven lines, labeled a–e (Table 2). Their energy positions and natural widths extracted from the fits are given in Table 3. Table 3 also shows a comparison with the results of Bari et al. [12] recorded with lower spectral resolution. The calculated XAS spectrum is shown in Figure 3b.

The XAS N1s spectrum of NH^+ is dominated by the peak centered at 398.91 eV (peak d) surrounded by three significant satellite bands (b), (c), and (e) centered at 397.87 eV, 398.31 eV, and 399.63 eV, respectively. We will tackle the identification and discussion of the resonance peaks in the order (b), (c), (e), and (d).

Table 3. Experimental position and natural width of the lines observed in the 394–401 eV photon energy region.

Line Label	Energy (eV)		Natural Width
	This Work	Reference [12] [1]	(meV)
a	394.81(6)	394.9	84(6)
b	397.87(5)	397.8	108(3)
c	398.31(6)	398.8	108(5)
c′	398.46(11)		
d	398.91(4)	398.8	142(20)
d′	399.25(5)		
e	399.63(5)	399.6	94(29)

[1] Uncertainty ± 0.1 eV.

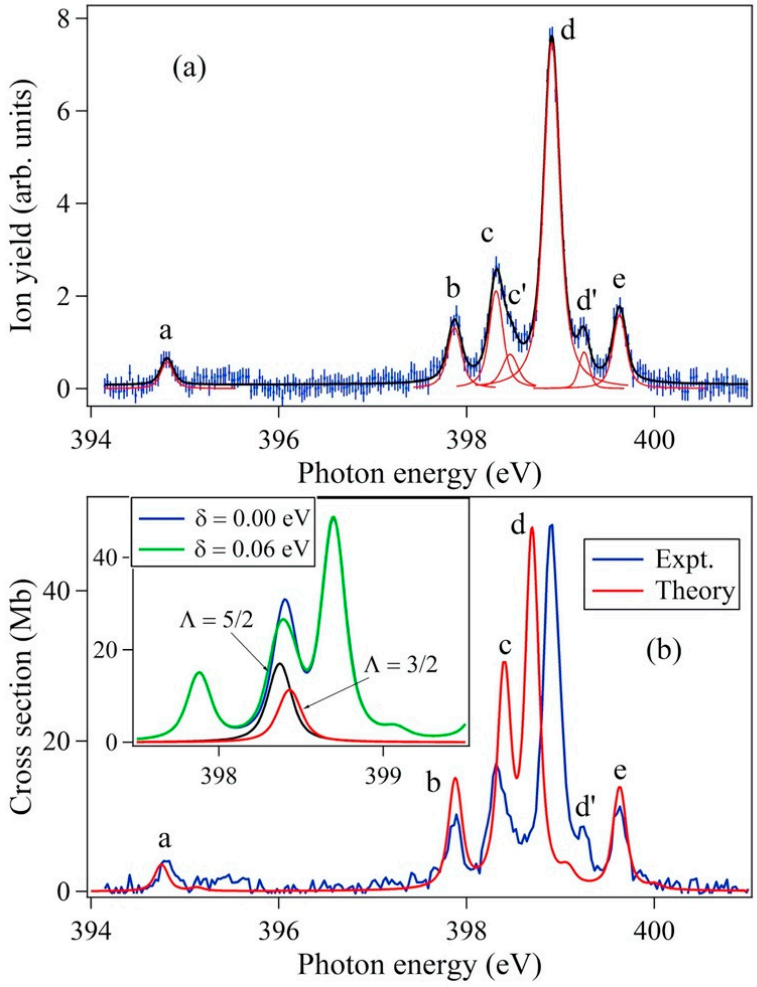

Figure 3. (**a**) Fitting by Voigt profiles of the experimental data, (**b**) NH+ experimental (blue trace Expt.) and calculated (red trace Theory) X-ray absorption spectra (XAS). The most important features are labeled (see Table 2). The experimental spectrum has been normalized to the maximum of peak d. In the insert is shown the splitting of the $^2\Delta$ states components (peak c) due to spin-orbit coupling for two δ values (see text).

Peak b $^4\Pi$

The first satellite line labeled b measured at 397.87 eV corresponds to a second high-spin quartet state associated with the degenerate $^4\Pi$ state involving final N1sσ^1 2σ^2 3σ^1 1π_x^2 1π_y^1/N1sσ^1 2σ^2 3$\sigma^1$1$\pi_x^1$1π_y^2 configurations. The DFT/B3LYP vertical core-excitation energy corresponds to the N1sσ^1 2σ^2 3σ^1 1π_x^1 1πy^1 →N1sσ^1 2σ^2 3σ^1 1π_x^2 1πy^1 and the transition energy is estimated to be 397.34 eV.

The equilibrium distance of the $^4\Pi$ adiabatic curve is very close (DFT 1.0919 Å, CI-SD 1.082 Å) to the internuclear distance found for the $^4\Sigma^-$ initial state. Hence, the N1s inner-shell vacancy does not considerably impact the NH bond length which experiences only a weak shortening of ≈0.01 Å, while the initial and final potential energy curves are found to be nearly parallel (see Figure 2). As a result, the Franck-Condon profile is limited to the v = 0 → v ′= 0 transition and no clear vibrational progression on the high-energy side of the peak at 397.8 eV is expected, as confirmed by the experiments. We note that the vibrational frequency is slightly reduced (CI-SD: 2557 cm^{-1}, DFT: 2516.7 cm^{-1}) compared to a $^4\Sigma^-$ (2716 cm^{-1}) and the anharmonicity coefficient $\omega_e x_e$ deduced from the PEC is ≈71 cm^{-1}. The differential zero-point energy correction (≈−0.01 eV) is rather small, and taking into account the relativistic correction of 0.2 eV, the DFT position of the peak b finally comes to 397.55 eV, i.e., only 2.8 eV above the $^4\Sigma^-$ final core-excited state and ≈−0.3 eV lower than the experimental energy position (397.87 eV). On the contrary, the CI-SD energy gap between the $^4\Sigma^-$ and the $^4\Pi$ core-excited states is rather overestimated (3.5 eV) vs the DFT value and the experiments (3.07 eV). In order to estimate the impact of correlation onto the gap, CI calculations including single up to triple excitations have been performed. As a result, the energy gap is significantly reduced from 3.5 to 3.13 eV, in very good agreement with the experimental value (3.07 eV). Hence, for easier comparison between theory and experiments in Figure 3b, we assumed a global shift (−0.35 eV) of the $^4\Pi$ and higher theoretical core-excited energies reported in Table 2. By this procedure, the $^4\Sigma^- \rightarrow {}^4\Pi$ theoretical transition (397.86 eV) reproduces the experimental excitation energy well (397.84 eV). The calculated oscillator strength is equal to 0.156 (see Table 2), corresponding to a strength of 17.1 Mb eV, so that the theoretical $^4\Sigma^-/^4\Pi$ intensity ratio (0.29) is in reasonable agreement with the measured experimental ratio between peaks area (0.33).

Peaks c $^2\Delta$ and e $^2\sum^+$

The peak labeled c on the spectrum is measured at 398.31 eV, i.e., lying 0.44 eV above the resonance b $^4\Pi$. This line is a superposition of two dipole-allowed degenerate doublet $^2\Delta$ states corresponding to the closed-shell N1sσ^1 2σ^2 3σ^2 1π_x ^{2} (or 1π_y^2) and open-shell N1sσ^1 2σ^2 3σ^2 1π_x^1 1π_y^1 core-excited configurations. The DFT/B3LYP vertical transition energy of the isolated doublet N1sσ^1 2σ^2 3σ^2 1π_x^2 configuration at the ground state NH^+ equilibrium distance (R = 1.077 Å) is calculated to be 398.62 eV. This value is slightly overestimated and differs more significantly (398.82 eV) with the experimental one when taking into account the relativistic correction (0.2 eV). The similar analysis developed by Bari et al. [12] for this resonance is confirmed by the present work.

In fact, the calculation of the $^2\Delta$ doublet core-excited energy is not as straightforward as for the single-configuration-like quartet lines, since two former closed-shell spin-doublet configurations (N1sσ^1 2σ^2 3σ^2 1π_x ^{2} (or 1π_y^2)) interact through the $J_{3p,3p}$ Coulomb integral, while the open-shell one consists of three different βαα(1), ααβ(2) and αβα (3) configuration spin-state functions, ultimately forming two doublet ($\frac{1}{\sqrt{6}}$(βαα(1) − 2 ααβ(2) + αβα(3)); $\frac{1}{\sqrt{2}}$αβα((3) − ααβ(2)) spin-adapted functions.

The origin of the $^2\Delta$ degeneracy is obvious from an analysis of the nature of the coupling matrix elements (Coulomb and exchange interactions) between the valence closed-shell N1sσ^1 2σ^2 3σ^2 1π $_x$ ^{2} (or 1π_y^2) and the three valence open shell N1sσ^1 2σ^2 3σ^2 1π_x^1 1π_y^1 configurations. For the former, let us basically consider a two-dimensional matrix (see Table 4) restricted to the 1π $_x$ ^{2} and 1π_y^2 valence-shell configurations. The diagonal terms $\langle$N1sα^1 2α^2 3α^2 1$\pi_{x(y)}{}^2$|H|N1sα^1 2α^2 3α^2 1$\pi_{x(y)}{}^2\rangle$ are identical, while the off-diagonal elements correspond to the Coulomb integral $J_{3p,3p}$ =

$\left\langle 3p_x(1)3p_y(2)\left|\frac{1}{r_{12}}\right|3p_x(1)3p_y(2)\right\rangle$ between two electrons localized on the nitrogen $3p_{x,y}$ atomic orbitals. This integral has been numerically estimated to be $\delta = 1.23$ eV. The trial diagonalization gives two energies, $\varepsilon'_1 = \varepsilon_1 - \delta$ and $\varepsilon'_2 = \varepsilon_1 + \delta$ and $\Delta = 2\delta = \varepsilon'_2 - \varepsilon'_1 \approx 1.46$ eV. The low-lying state (ε'_1) belongs to a $^2\Delta$ spectroscopic term while the upper one (ε'_2) belongs to a $^2\Sigma^+$ state symmetry. Using a larger CI space of configurations, it is interesting to note that the valence closed shell $1\sigma_1^2 2\sigma^2 3\sigma^2 1\pi_x^2 \pi_y^0$ ($1\pi_x^0 \pi_y^2$) configurations substantially correlate with $1\sigma_1^1\ 2\sigma^2 3\sigma^0 3p_x^2 3p_y^2$, where two electrons contribute to fill the $3p_{x,y}$ orbitals. This interaction of configurations reduces the Δ energy gap to ≈1.2 eV, which roughly corresponds to the energy difference (1.29 eV) between peaks c $^2\Delta$ and e $^2\sum^+$ (Table 3). To conclude this part, peak e is therefore attributed to the ($^2\Pi$) $N1s^2\ 2\sigma^2\ 3\sigma^2\ 1\pi_x^1$ ($1\pi_y^1$) → ($^2\Sigma^+$) $N1s^1\ 2\sigma^2\ 3\sigma^2\ 1\pi_x^2$ (or $1\pi_y^2$).

Table 4. Diagonal (ε) and sub-diagonal coupling matrix elements between the $N1s\sigma^1 1\pi_x^a 1\pi_y^b$ (a = 0 or 1; b = 0 or 1) configurations. β and α denote spin configurations. For example, βαα means $\overline{N_{1s^1}}\ \pi_x^1\ \pi_y^1$. J is a Coulomb matrix element. K is a (positive) exchange matrix element.

$N1s\sigma^1$	$1\pi_x^2$	$1\pi_y^2$	βαα	ααβ	αβα
$1\pi_x^2$	$\varepsilon_{\pi_{x^2}}$	$J_{3p,3p}$	0	0	0
$1\pi_y^2$	$J_{3p,3p}$	$\varepsilon_{\pi_{y^2}} = \varepsilon_{\pi_{x^2}}$	0	0	0
βαα	0	0	$\varepsilon_{\beta\alpha\alpha}$	$-K_{1s,3p}$	$-K_{1s,3p}$
ααβ	0	0	$-K_{1s,3p}$	$\varepsilon_{\alpha\alpha\beta}$	$-K_{3p,3p}$
αβα	0	0	$-K_{1s,3p}$	$-K_{3p,3p}$	$\varepsilon_{\alpha\beta\alpha} = \varepsilon_{\alpha\alpha\beta}$

Transition and results from configuration interaction effects: The corresponding calculated CI-SD oscillator strength is found to be 0.038, i.e., 4.17 Mb eV strength. There are three different spin-configurations, denoted βαα (1), ααβ (2), and αβα (3) for the $N1s\sigma^1\ 2\sigma^2\ 3\sigma^2\ 1\pi_x^1\ 1\pi_y^1$ configuration. The spin configuration (1) differs from (2) and (3) since for the former, the two valence electrons have the same (α) spin, leading to spin-dependent diagonal matrix elements. As a result, the coupling matrix element between (1) and (2)/(3) corresponds to the negative of the exchange integral $K_{1s,3p} = \left\langle 1s(1)3p_{x(y)}(2)\left|\frac{1}{r_{12}}\right|1s(2)3p_{x(y)}(2)\right\rangle = 1.38$ eV.

The coupling matrix between (2) and (3) corresponds to the negative of the exchange integral $K_{3p,3p} = \left\langle 3p_x(1)3p_y(2)\left|\frac{1}{r_{12}}\right|3p_x(2)3p_y(1)\right\rangle$, where $K_{3p,3p} = J_{3p,3p}$.

In the spin-adapted space, the 3 × 3 matrix can be compacted to a 2 × 2 matrix form. The diagonalization gives two eigenvalues (ε''_1 and ε''_2). The energy gap $\delta'' = \varepsilon''_2 - \varepsilon''_1$ is found equal to ≈0.3 eV. The spin function associated with the eigenstate with the ε''_1 eigenvalue is constructed with 75% of the $\frac{1}{\sqrt{6}}(\beta\alpha\alpha(1) - 2\ \alpha\alpha\beta(2) + \alpha\beta\alpha(3))$ spin-function and 25% of the $\frac{1}{\sqrt{2}}(\alpha\beta\alpha(3) - \alpha\alpha\beta(2))$ one. Comparing the values, we found that $\varepsilon''_1 = \varepsilon'_1$, both states forming the so-called $^2\Delta$ spectroscopic term, and the corresponding calculated oscillator strengths are similar and each equal to 0.04 (4.35 Mb eV) (see Table 2).

The vertical energy position at the $^2\Pi$ equilibrium distance (1.065 Å) of the $^2\Delta$ band c is finally determined by adding the vertical energy difference between the $^4\Sigma^-$ core-excited state (394.83 eV) and the $^2\Pi$ initial state to the CI-SD vertical energy gap between the $^4\Pi$ and $^4\Sigma^-$ core-excited states (3.17 eV), plus the $^2\Delta$-$^4\Pi$ energy gap (+0.4 eV) extract from the PEC analysis. Following this procedure, the $^2\Delta$ transition energy is finally estimated to be ~398.40 eV while the $^2\sum^+$ transition energy is estimated to be ~399.63 eV, in reasonable agreement with the experiment.

Interestingly, peak c features a pronounced asymmetrical profile, on the high photon energy side. This is particularly intriguing since (see Figure 2) the $^2\Delta$ CI-SD adiabatic potential energy curves have a similar global minimum (R_{min}) at 1.032 Å, thus the NH bond is shrunk by only –0.032 Å from the $^2\Pi$ ($N1s^2\ 2\sigma^2\ 3\sigma^2\ 1\pi_x^1\ 1\pi_y^0$ or $1\pi_x^0\ 1\pi_y^1$) initial state. The PEC of the ($N1s^2\ 2\sigma^2\ 3\sigma^1\ 1\pi_{x(y)}^2\ 1\pi_{y(x)}^0$) $^2\Delta$ configuration presents a characteristic anharmonic behavior with fundamental vibrational frequency, ω_e, and anharmonicity constant, $\omega_e x_e$, equal to 3250 and 120 cm^{-1}, respectively. The Franck-Condon envelope consists mainly (97 %) of the v = 0 → v′ = 0 vibrational transition with a weak contribution

(3%) of v = 0 → v′ = 1 at 0.38 eV from the main band, which may account for the structure labeled *c*′ in Figure 3a. For the second $^2\Delta$ state corresponding to the N1s^1 2σ^2 3σ^2 1π$_x^1$ 1π$_y^1$ configuration, the PEC is parallel to the former $^2\Delta$ state in the 1–1.6 Å range of interatomic distances and shows two regions at 1.6 Å and 2.0 Å, where the curve crosses with other electronic states. However, the Franck-Condon profile is very similar to that found above, i.e., (97%) of the v = 0 → v′ = 0 vibrational transition with a weak contribution (3%) of v = 0 → v′ = 1 at 0.38 eV from the main band, which contributes to enhance the peak c.

We suggest a spin-orbit (SO) coupling effect between the two $^2\Delta$ (S = 1/2, Λ = 2) doublet states as the cause for this wide asymmetric profile. To support this, we have carried out CI-SD + SO calculations limited to the N1s^1 2σ^2 3σ^2 1π$_x^1$ 1π$_y^1$ and N1s^1 2σ^2 3σ^2 1π$_x^2$ (π$_y^0$) configurations. The spin-orbit coupling thus lifts the degeneracy between the two $^2\Delta$ states and the calculations yield the two J$_z$ = 5/2 and J$_z$ = 3/2 SO components in the 3:2 statistical ratio. The corresponding energy gap (δ_{SO}) is theoretically estimated to ~0.02 eV, the value of which appears somewhat underestimated. To illustrate this (see insert in Figure 3b), we have simulated the 394–400 eV energy region considering two different values of δ_{SO} (0.00 eV, 0.06 eV). As observed, the asymmetric tail of peak c to the high photon energy region is reasonably reproduced when the spin-orbit coupling effect is taken into account.

Peak d $^2\Sigma^-$

The main peak labeled d on the spectrum corresponds to the $^2\Sigma^-$ state with the final N1sσ^1 2σ^2 3σ^2 1π$_x^1$ 1π$_y^1$ electronic configuration. The associated oscillator strength is calculated to be 0.121. The corresponding spin function is built with contributions of 75% and 25% from the $\frac{1}{\sqrt{2}}(\alpha\beta\alpha(3) - \alpha\alpha\beta(2))$ and $\frac{1}{\sqrt{6}}(\beta\alpha\alpha(1) - 2\alpha\alpha\beta(2) + \alpha\beta\alpha(3))$ spin-adapted configurations, respectively. Analyzing the potential energy curves displayed in Figure 2, the energy difference between $^2\Sigma^-$ and $^2\Delta$ at the initial $^2\Pi$ interatomic distance is nearly 0.40 eV, so that the corresponding transition energy is 398.80 eV, in good agreement with the recorded experimental value of 398.91 ± 0.04 eV. As observed, the PEC is nearly parallel to $^2\Delta$. The vibration frequency value is similar to that of $^2\Delta$, where ω_e (b $^2\Delta$) = 3250 cm^{-1}. The Franck-Condon envelope associated with the $^2\Sigma^-$ state consists, as for $^2\Delta$, of two components with 0.96 and 0.03 relative intensities for the v = 0 → v′ = 0 and v = 0 → v′ = 1 transitions, respectively. Due to the high intensity of peak d, the vibrational component v = 0 → v = 1 (labeled d′) is clearly detectable on the theoretical spectrum and also observed experimentally.

To achieve agreement between the first quartet line $^4\Sigma^-$ at 394.81 eV and peak d $^2\Sigma^-$ theoretical cross-sections with the experimental data, the relative populations of the $^2\Pi$ and $^4\Sigma^-$ lower states have to be taken into account. A scaling factor of ~0.5 was applied to the quartet states' theoretical data, bringing a satisfactory accord between theory and experiment. Considering the experimental energy gap (ΔE = 0.071 eV) between the $^2\Pi$ and $^4\Sigma^-$ electronic ground states, this factor would correspond to an equivalent source plasma equilibrium temperature of ~600 K, although it is realized that temperature may not be a good physical concept in this case.

4.2.3. Region 400–430 eV

The experimental spectrum is compared to the calculated XAS spectrum on Figure 4. It presents unresolved broad structures above 405 up to 430 eV. As reported in Table 2, the most intense lines are mainly due to the excitation of a 1s electron, from the initial doublet $^2\Pi$ or quartet $^4\Sigma^-$ states, to the first low-lying empty orbitals (for example 4σ, 2π) to form Rydberg series, converging on various 1s ionization thresholds ranging between 425 and 430 eV with singlet, triplet, and quintet spin state configurations. The calculated energy position of these thresholds is shown in the top right corner of Figure 4 and more theoretical details are given in Table 5. As indicated by the theory in Table 2, the two most intense lines (labeled f) are close, lying in the 409–412 eV energy region. The first $^4\Sigma^-$ state f lying at 409.04 eV corresponds to a multiple excitation, i.e., 1σ^{2}2σ^{2}3σ^{1}1π$_x^1$1π$_y^1$ → 1σ^{1}2σ^{1}3σ^{2}1π$_x^1$1π$_y^1$4σ^1 transition, where a N1s inner-shell electron is promoted simultaneously with an inner-valence electron (2σ) to doubly fill the 3σ and partially fill the 4σ shell. The second $^2\Pi$

state lying at 412.17 eV corresponds to the $1\sigma^2 2\sigma^2 3\sigma^2 1\pi_{x(y)}{}^1 \rightarrow 1\sigma^1 2\sigma^2 3\sigma^2 1\pi_{x(y)}{}^1 4\sigma^1$ transition, where the N1s inner-shell electron is directly promoted to the 4σ shell. Their oscillator strengths are 0.0332 and 0.0261 respectively, corresponding to strengths of 3.64 and 2.86 Mb eV. Comparing the oscillator strength values reported in Table 2, these two lines are expected to be of similar intensities to peaks within the energy region between 397 and 401 eV.

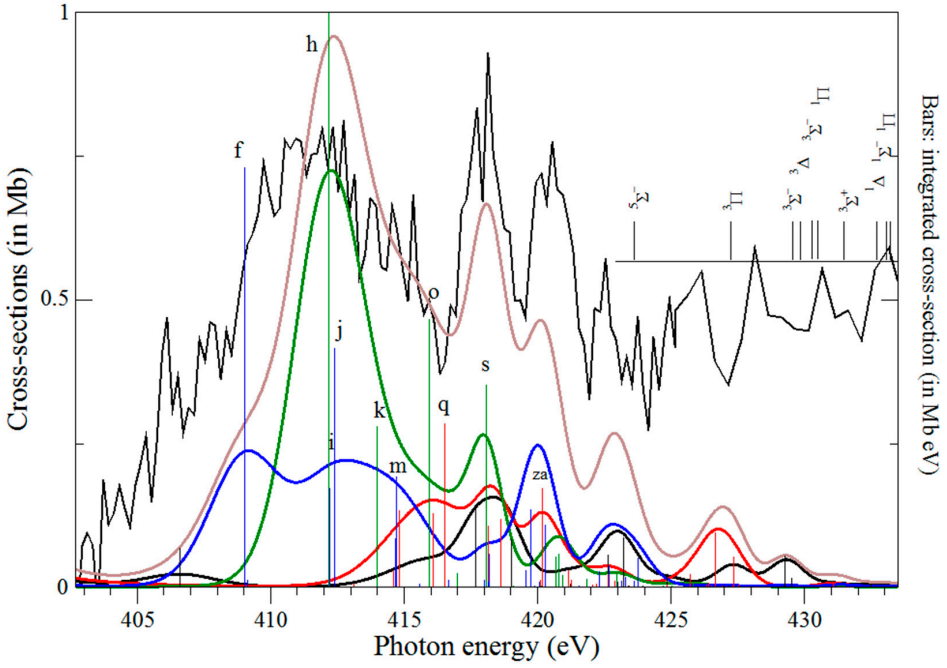

Figure 4. Experimental and simulated spectra in the energy region between 407 and 430 eV. Blue lines/bars: Quartet $^4\Sigma^-$ and $^4\Pi$ states (quartet cross-sections were scaled by a factor of 0.5 to take into account source population effects (see discussion in text)). Green lines: $^2\Pi$ states. Red lines/bars: $^2\Sigma^-$ and $^2\Delta$ states. Black lines/bars: $^2\Sigma^+$ and $^2\Delta$ states. Cross-sections are given in Mb. Bars: Integrated cross-section under the peaks (in Mb eV). Experimental intensities were divided by a factor of eight (see text). The calculated energy positions of the ten lowest lying ionization thresholds are shown in the top right corner.

Table 5. First ten low-lying $N1s^{-1}$ vertical ionization energies calculated at the configuration interaction single and double substitutions (CI-SD) level of theory. *Absolute density functional theory (DFT) triplet ($^2\Pi \rightarrow {}^3\Pi$) and quintet ($^4\Sigma^- \rightarrow {}^5\Sigma^-$) $N1s^{-1}$ vertical ionization energies at R_D = 1.077 Å and R_Q = 1.113 Å respectively, taking into account relativistic corrections (0.2 eV), were used as references. For each final state, the contributions of the main configurations are given in parentheses (%).

Threshold Number	Absolute Energy (eV)	State	Main Configurations
1	423.61 *	$(^5\Sigma^-)_Q$	$1\sigma^1 2\sigma^2 3\sigma^1 1\pi_x{}^1 1\pi_x{}^1$ (97.4)
2	426.93 *	$(^3\Pi)_D$	$1\sigma^1 2\sigma^2 3\sigma^2 1\pi_{x,y}{}^1$
3	429.39	$(^3\Sigma^-)_Q$	$1\sigma^1 2\sigma^2 3\sigma^1 1\pi_x{}^1 1\pi_y{}^1$ (75.6)
4	429.52	$(^3\Delta)_Q$	$1\sigma^1 2\sigma^2 3\sigma^1 1\pi_x{}^1 1\pi_y{}^1$(8.1)/$1\sigma^1 2\sigma^2 3\sigma^1 1\pi_x{}^2$(43.8)/$1\sigma^1 2\sigma^2 3\sigma^1 1\pi_y{}^2$(43.8) $1\sigma^1 2\sigma^2 3\sigma^1 1\pi_x{}^1 1\pi_y{}^1$(87.6)/$1\sigma^1 2\sigma^2 3\sigma^1 1\pi_x{}^2$(4.05)/$1\sigma^1 2\sigma^2 3\sigma^1 1\pi_y{}^2$(4.05)
5	429.95	$(^3\Sigma^-)_Q$	$1\sigma^1 2\sigma^2 3\sigma^1 1\pi_x{}^1 1\pi_x{}^1$ (96.2)
6	430.22	$(^1\Pi)_D$	$1\sigma^1 2\sigma^2 3\sigma^2 1\pi_{x,y}{}^1$
7	431.23	$(^3\Sigma^+)_Q$	$1\sigma^1 2\sigma^2 3\sigma^1 1\pi_x{}^2$(46.0) $1\sigma^1 2\sigma^2 3\sigma^1 1\pi_y{}^2$(46.0)
8	432.43	$(^1\Delta)_Q$	$1\sigma^1 2\sigma^2 3\sigma^1 1\pi_x{}^2$(42.0) $1\sigma^1 2\sigma^2 3\sigma^1 1\pi_y{}^2$(42.0)/$1\sigma^1 2\sigma^2 3\sigma^1 1\pi_x{}^1 1\pi_x{}^1$(8.6) $1\sigma^1 2\sigma^2 3\sigma^1 1\pi_x{}^1 1\pi_x{}^1$(84.0)/ $1\sigma^1 2\sigma^2 3\sigma^1 1\pi_x{}^2$(4.3) $1\sigma^1 2\sigma^2 3\sigma^1 1\pi_y{}^2$(4.3)
9	432.79	$(^1\Sigma^-)_Q$	$1\sigma^1 2\sigma^2 3\sigma^1 1\pi_x{}^1 1\pi_y{}^1$ (91.1)
10	432.87	$(^1\Pi)_Q$	$1\sigma^1 2\sigma^2 3\sigma^0 1\pi_x{}^1$ $1\pi_y{}^2$(58.7)/ $1\sigma^1 2\sigma^2 3\sigma^0 1\pi_x{}^2 1\pi_y{}^1$(23.9) $1\sigma^1 2\sigma^2 3\sigma^0 1\pi_x{}^2$ $1\pi_y{}^1$(58.7)/ $1\sigma^1 2\sigma^2 3\sigma^0 1\pi_x{}^1 1\pi_y{}^2$(23.9)

This picture contrasts with the experimental observation which instead shows an unresolved plateau. As displayed in Figure 2, both the PECs associated with the region f clearly present dissociative profiles. For instance, the gradient along the steepest descent (~12.5 eV/Å) at the $^2\Pi$ equilibrium distance is large, and the width of the Franck-Condon profile is estimated to be 2.3 eV. For the $^4\Sigma^-$ state, the gradient is even larger (~16.5 eV/Å) and the energy width of the Franck-Condon profile is estimated to be 3.1 eV.

At higher energies, near 420 eV of photon energy, the spectrum also reveals a number of broad features. The PECs for this energy region have not been explicitly computed. We can assume that high-energy Rydberg core-excited states should present similar behavior as core-ionized states. As a showcase, the DFT numerical gradients F_{NH} were carried out for the triplet ($^3\Pi$, N1s^1 2σ^2 3σ^2 1π$_x$^{1}) and quintet ($^5\Sigma^-$, N1s^1 2σ^2 3σ^1 1π$_x$^{1}1π$_y$^{1}) core-ionized molecular bications, from the formula

$$F_{\nu_{NH}} = \left.\frac{\partial U}{\partial Q_{NH}}\right|_e = \sqrt{\mu_{\nu_{NH}}} \sum_{j=1}^{3N} \frac{A_j^{\nu_{NH}}}{\sqrt{m_j}} \left.\frac{\partial U}{\partial R_j}\right|_e \quad (6)$$

where the gradient $F\nu_{NH}$ is the partial derivative of the final state potential energy surface along the unique stretching normal mode, calculated at the equilibrium geometry, and $A_j^{\nu_{NH}}$ is the output GAMESS (US) column vector of the unitary transformation matrix between the mass weighted Cartesian and normal coordinates for the corresponding mode. As a result, we found $F_{\nu_{NH}}^{^3\Pi}$ = 4.9 eV/Å and $F_{\nu_{NH}}^{^5\Sigma^-}$ = 6.0 eV/Å respectively, corresponding to Gaussian envelopes with FWHMs equal to 0.83 and 1.13 eV. As reported in Table 2, the various spin-state core-ionization thresholds lie over a wide energy range (426–430 eV). In order to simulate the 401–430 experimental energy region of spectrum, we assumed a large FWHM of 2.5 eV for core-excited states lying between 401 and 417 eV and a FWHM of 1.0 eV for core-excited states lying between 417 eV and the ionization thresholds. As observed in Figure 4, the overall shape of the experimental spectrum is fairly well reproduced by theory. However, once the experimental spectrum is normalized to theory on the maximum of peak d, as performed in Figure 3b, the spectral intensity in the energy region 405–430 eV is greater than that of the theoretical spectrum by a factor of 8. One explanation for this discrepancy is that, while theory calculates the absorption spectrum, experiment measures only the N^{2+} fragmentation channel following the creation of the 1s hole. Our results seem to indicate that the relative probability of producing the N^{2+} fragment is higher in the region 405–430 eV than in the region 395–401 eV. A similar argument was proposed by Bari et al. [12] to explain the discrepancy between their theoretical and experimental results. They also observed relative intensity differences between the low- and high-energy regions of their spectra but in their case, by a lower factor of ≈1.8. We also note that the N-K absorption spectrum of NH^+ is characterized by a collection of ionization thresholds extending over more than 10 eV. The low-lying ionization threshold corresponds to ejection of one N1s electron from the $^4\Sigma^-_{(Q)}$ quartet initial state (1σ^{2}2σ^{2}3σ^{1}1π$_x$^{1}1π$_x$^{1}) to form the $^5\Sigma^-_{(Q)}$ state with the 1σ^{1}2σ^{2}3σ^{1}1π$_x$^{1}1π$_x$^{1} open-shell configuration. These direct N1s photoionization processes, contributing to the experimental spectrum of Figure 1a as a more or less constant signal above 425 eV, are not included in the present calculations.

5. Conclusions

We have studied both experimentally and theoretically the excited states of the NH^+ molecular ion by focusing on the N1s inner-shell photo-absorption spectrum in the photon energy region 390–450 eV. The experiments used an ECR plasma molecular ion source coupled with monochromatized synchrotron radiation in a merged-beam configuration. The experimental spectrum was obtained by detection of the N^{2+} photofragments. The photon bandwidth was narrow enough to partially resolve the vibrational distributions in the 1s → π* transitions. The interpretation of the experimental spectrum was undertaken based on a comparison with the total photo-absorption cross-sectional profiles

calculated using ab-initio configuration interaction theoretical methods inclusive of spin-orbit coupling and vibrational dynamics.

Author Contributions: Conceptualization, J.-M.B., D.C., S.G., J.-P.M., and E.T.K.; methodology, E.S., D.C., J.-M.B., J.-P.M., B.M., and E.T.K.; software, S.C., B.M., and D.C.; validation, J.-P.M., D.C., J.-M.B., E.S., and E.T.K.; formal analysis, J.-P.M., E.S., J.M.B., E.T.K., and S.C.; investigation, J.-M.B., J.-P.M., E.T.K., S.C., and E.S.; resources, S.C. and J.-M.B.; data curation, S.G.; writing—original draft preparation, S.C., J.M.B., J.-P.M., and B.M.; writing—review and editing, S.C., J.-M.B., J.-P.M., and E.T.K.; visualization, J.-M.B. and S.C. All authors have read and agreed to the published version of the manuscript.

Funding: This research received no external funding.

Acknowledgments: The authors would like to thank SOLEIL for the award of beamtime and the SOLEIL staff J. Bozek, C. Nicolas, and A. Milosavljevic for assistance in using the PLEIADES beamline. E.K., B.M.L., and J.-P.M. would like to thank SOLEIL for financial help with accommodation and subsistence during beamtime.

Conflicts of Interest: The authors declare no conflict of interest.

References

1. Gerin, M.; Neufeld, D.A.; Goicoechea, J.R. Interstellar Hydrides. *Annu. Rev. Astron. Astrophys.* **2016**, *54*, 181–225. [CrossRef]
2. Rednyk, S.; Roucka, Š.; Kovalenko, A.; Tran, T.D.; Dohnal, P.; Plašil, R.; Glosík, J. Reaction of NH^+, NH_2^+, and NH_3^+ ions with H_2 at low temperatures. *Astron. Astrophys.* **2019**, *625*, A74. [CrossRef]
3. Le Gal, R.; Hily-Blant, P.; Faure, A.; Pineau des Forêts, G.; Rist, C.; Maret, S. Interstellar chemistry of nitrogen hydrides in dark clouds. *Astron. Astrophys.* **2014**, *562*, A83. [CrossRef]
4. Wagenblast, R.; Williams, D.A.; Millar, T.J.; Nejad, L.A.M. On the origin of NH in diffuse interstellar clouds. *Mon. Not. R. Astron. Soc.* **1993**, *260*, 420–424. [CrossRef]
5. Amero, J.M.; Vazquez, G.J. Electronic Structure of NH^+: An Ab Initio Study. *Int. J. Quantum Chem.* **2005**, *101*, 396–410. [CrossRef]
6. Chen, C.T.; Ma, Y.; Sette, F. *K*-shell photoabsorption of the N_2 molecule. *Phys. Rev. A* **1989**, *40*, 6737. [CrossRef]
7. Mosnier, J.-P.; Kennedy, E.T.; Van Kampen, P.; Cubaynes, D.; Guilbaud, S.; Sisourat, N.; Puglisi, A.; Carniato, S.; Bizau, J.-M. Inner-shell photoexcitations as probes of the molecular ions CH^+, OH^+, and SiH^+: Measurements and theory. *Phys. Rev. A* **2016**, *93*, 061401. [CrossRef]
8. Kennedy, E.T.; Mosnier, J.-P.; Van Kampen, P.; Bizau, J.M.; Cubaynes, D.; Guilbaud, S.; Carniato, S.; Puglisi, A.; Sisourat, N. Evolution of L-shell photoabsorption of the molecular-ion series SiH^{n+} (n = 1,2,3): Experimental and theoretical studies. *Phys. Rev. A* **2018**, *97*, 043410. [CrossRef]
9. Klumpp, S.; Guda, A.A.; Schubert, K.; Mertens, K.; Hellhund, J.; Müller, A.; Schippers, S.; Bari, S.; Martins, M. Photoabsorption of the molecular IH cation at the iodine 3d absorption edge. *Phys. Rev. A* **2018**, *97*, 033401. [CrossRef]
10. Lindblad, R.; Kjellsson, L.; Couto, R.C.; Timm, M.; Bülow, C.; Zamudio-Bayer, V.; Lundberg, M.; Von Issendorff, B.; Lau, J.T.; Sorensen, S.L.; et al. X-ray Absorption Spectrum of the N_2^+ Molecular Ion. *Phys. Rev. Lett.* **2002**, *124*, 203001. [CrossRef]
11. Couto, R.C.; Kjellsson, L.; Ågren, H.; Carravetta, V.; Sorensen, S.L.; Kubin, M.; Bülow, C.; Timm, M.; Zamudio-Bayer, V.; von Issendorff, B.; et al. The carbon and oxygen K-edge NEXAFS spectra of CO^+. *Phys. Chem. Chem. Phys.* **2020**, *22*, 16215–16223. [CrossRef] [PubMed]
12. Bari, S.; Inhester, L.; Schubert, K.; Mertens, K.; Schunck, J.O.; Dörner, S.; Deinert, S.; Schwob, L.; Schippers, S.; Müller, A.; et al. Inner-shell X-ray absorption spectra of the cationic series NH_y^+ (y = 0–3). *Phys. Chem. Chem. Phys.* **2019**, *21*, 16505–16514. [CrossRef] [PubMed]
13. Bizau, J.M.; Cubaynes, D.; Guilbaud, S.; El Hassan, N.; Al Shorman, M.M.; Bouisset, E.; Guigand, J.; Moustier, O.; Marié, A.; Nadal, E.; et al. A merged-beam setup at SOLEIL dedicated to photoelectron–photoion coincidence studies on ionic species. *J. Electron Spectrosc. Relat. Phenom.* **2016**, *210*, 5–12. [CrossRef]
14. Gharaibeh, M.F.; Bizau, J.M.; Cubaynes, D.; Guilbaud, S.; El Hassan, N.; Al Shorman, M.M.; Miron, C.; Nicolas, C.; Robert, E.; Blancard, C.; et al. K-shell photoionization of singly ionized atomic nitrogen: Experiment and theory. *J. Phys. B At. Mol. Opt. Phys.* **2011**, *44*, 175208. [CrossRef]

15. Becke, A.D. Density-functional thermochemistry. III. The role of exact exchange. *J. Chem. Phys.* **1993**, *98*, 5648–5652. [CrossRef]
16. Lee, C.; Yang, W.; Parr, R.G. Development of the Colle-Salvetti correlation-energy formula into a functional of the electron density. *Phys. Rev. B* **1988**, *37*, 785–789. [CrossRef] [PubMed]
17. Schmidt, M.W.; Baldridge, K.K.; Boatz, J.A.; Elbert, S.T.; Gordon, M.S.; Jensen, J.H.; Koseki, S.; Matsunaga, N.; Nguyen, K.A.; Su, S.; et al. Montgomery, General atomic and molecular electronic structure system. *J. Comput. Chem.* **1993**, *14*, 1347–1363. [CrossRef]
18. Prince, K.C.; Vondráček, M.; Karvonen, J.; Coreno, M.; Camilloni, R.; Avaldi, L.; de Simonel, M. A critical comparison of selected 1s and 2p core hole widths. *J. Electron Spectrosc. Relat. Phenom.* **1999**, *101*, 141–147. [CrossRef]
19. Woon, D.E.; Dunning, T.H. Gaussian basis sets for use in correlated molecular calculations. V. Core-valence basis sets for boron through neon. *J. Chem. Phys.* **1995**, *103*, 4572–4585. [CrossRef]
20. Colin, R. Perturbations between the $X^2\Pi$ and $a^4\Sigma^-$ states of the NH^+ ion. *J. Mol. Spec.* **1989**, *136*, 387–401. [CrossRef]
21. Feller, D.; Sordo, J.A. A CCSDT study of the effects of higher order correlation on spectroscopic constants. I. First row diatomic hydrides. *J. Chem. Phys.* **2000**, *112*, 5604–5610. [CrossRef]
22. Wilson, D.L. Λ-type doubling in the molecules $^{14}NH^+$, $^{15}NH^+$, and $^{14}ND^+$. *Mol. Phys.* **1978**, *36*, 597–610. [CrossRef]